RSC Advances

PAPER

View Article Online
View Journal | View Issue

Cite this: *RSC Adv.*, 2018, **8**, 30055

Nopinone-based aggregation-induced emission (AIE)-active difluoroboron β-diketonate complex: photophysical, electrochemical and electroluminescence properties†

Qian Jiang,[a] Mingguang Zhang,[a] Zhonglong Wang,[a] Jie Song,[b] Yiqin Yang,[ac] Wenchao Li,[d] Wen Gu,[ac] Xu Xu,*[ac] Haijun Xu*[ac] and Shifa Wang *[ac]

Received 12th June 2018
Accepted 14th August 2018

DOI: 10.1039/c8ra05031g

rsc.li/rsc-advances

Four difluoroboron (BF_2) β-diketonate nopinone complexes **3a–3d** that exhibited typical aggregation-induced emission (AIE) properties were synthesized using the natural renewable β-pinene derivative nopinone as the starting material. The thermal, photophysical, electrochemical and electroluminescent properties as well as the AIE properties of complexes **3a–3d** were analyzed systematically. The data of photophysical and electrochemical demonstrated that compound **3b** with a methoxy group exhibited the largest bathochromic shift, the highest absolute photoluminescence quantum yields and narrowest optical bandgap among **3a–3d**. Using **3b** as the emitter, electroluminescent (EL) device **I** exhibits blue-green light with CIE coordinates of (0.2774, 0.4531) and showed a better performance with a luminous efficacy (η_p) of 7.09 lm W^{-1} and correlated color temperature (T_C) of 7028 K. The results demonstrate that new AIE compounds are promising solid-state luminescent materials with practical utility in electroluminescent materials.

1. Introduction

In recent years, organoboron complexes as the most important type of fluorescent dyes,[1,2] have caused great interest. Difluoroboron (BF_2) complexes based on N- and O-donor ligands are known to show intense fluorescence in solution and solid state.[3,4] Besides, they have outstanding fluorescence properties such as high quantum yield, large stokes shifts, intense emission, thermal and photochemical stability.[5–8] These features have been exploited in NIR[9,10] and molecular probes,[11] optical imaging,[12,13] solar cells,[14] oxygen[15] and mechanical sensors,[16,17] laser dyes,[18] anion receptors[19,20] and organogels.[21] For example, some difluoroboron (BF_2) β-diketonate complexes showed mechanochromic luminescence.[22] In 2015, some new difluoroboron complexes were reported as biological oxygen sensors.[23,24]

Traditional luminophores generally suffer from the aggregation-caused quenching (ACQ) effect, which reduced the performance of traditional luminophores when used in optoelectronic devices. In 2001, Tang discovered the phenomenon of aggregation-induced emission (AIE): luminophores show non-fluorescent in solutions, but highly emissive in aggregate formation or in crystalline state.[25] The main cause of the AIE effects is restriction of intramolecular motions (RIM), including rotation and vibration along the C–C single bond.[26] Many fluorescent organic dyes showing AIE properties are studied, they include tetraphenylethene,[27,28] siloles,[29–31] BODIPY dyes,[32,33] triphenylethene,[34,35] tetraphenyl-1,4-butadiene (TPBD),[36] pentacenequinone[37] and isophorone[38] based dyes. Recently, the exploration of new AIE fluorophores is still a challenging field to synthetic chemist. In this paper, a simple strategy to synthesize high-performance solid-state light emitters with AIE property is proposed.

As a rich and cheap plant essential oils, the annual output of turpentine is about 100 000 tons or more. Nopinone is a derivative synthesized from β-pinene, which is a main ingredient of turpentine. In recent years, many nopinone derivatives have been synthesized such as 3-cyanopyridine derivatives,[39] chiral 1,3-aminoalcohols and 1,3-diols,[40] terpenyl diselenides,[41] quinazolin-2-amine nopinone derivatives.[42] However, there is no work about using the pinane frame to construct some new EL materials.

In this paper, we designed and synthesized four novel nopinone derivatives-containing difluoroboron β-diketonate groups. The synthetic route is illustrated in Scheme 1. The structures of these compounds are characterized with ^{1}H NMR,

[a]College of Chemical Engineering, Nanjing Forestry University, Nanjing, 210037, P. R. China
[b]Department of Chemistry and Biochemistry, University of Michigan-Flint, Flint, MI 48502, USA
[c]Co-Innovation Center of Efficient Processing and Utilization of Forest Resources, Nanjing Forestry University, Nanjing, 210037, P. R. China
[d]Sinofert, Sinochem Group, Beijing, 100031, P. R. China

† Electronic supplementary information (ESI) available. CCDC 1848721. For ESI and crystallographic data in CIF or other electronic format see DOI: 10.1039/c8ra05031g

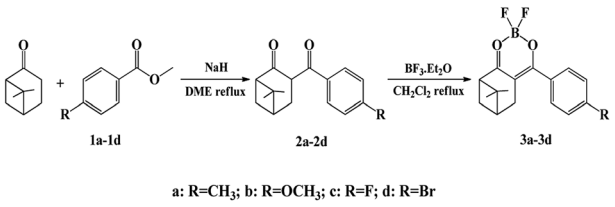

Scheme 1 Synthetic route of compounds **3a–3d**.

^{13}C NMR, HRMS and X-ray analyses. The thermal, photophysical, electrochemical properties, and molecular orbital distribution of four new fluorescent compounds are also investigated. Finally, two of them have been successfully applied to electroluminescent devices. This is the first report of nopinone-based fluorescent compounds for electroluminescence materials application.

2. Experimental

2.1. Materials and measurements

Reagents and solvents were purchased from commercial suppliers and used without further purification. Mass spectra were carried out on an America Agilent 5975c mass spectrometer. The ^{1}H NMR and ^{13}C NMR spectra were recorded in $CDCl_3$ solutions on a Bruker AV 400 spectrometer. Melting points were performed with an X-6 microscopic melting point apparatus. UV-visible absorption spectra were investigated by PerkinElmer Lambda 950. PL emission spectra were investigated by PerkinElmer LS55 fluorescence spectrophotometer scan from 320 nm to 600 nm with a 100 nm min^{-1} of scan speed. Thermogravimetric analysis (TGA) was carried out on a TGA 2050 thermogravimetric analyzer under nitrogen at a heating rate of 10 °C min^{-1}, and T_d was reported as the temperatures at 5% weight losses. Cyclic voltammetry was taken on a CHI-600E electrochemical analyzer. The measurements were determined using a conventional three-electrode configuration consisting of a glassy carbon working electrode, a platinum wire auxiliary electrode and an Ag/AgCl reference electrode, the scan rate was 10 mV s^{-1}. Fluorescence lifetimes were taken on a steady and transient state fluorometer (Quantaurus-Tau, C11367). The absolute photoluminescence quantum yield (Φ_{PL}) was measured with a Hamamatsu absolute PL quantum yield spectrometer equipped (Quantaurus-QY, C11347). X-ray data were collected on a Bruker D8 Venture area diffractometer.

2.2. Fabrication of electroluminescent (EL) devices and testing

Devices was fabricated by embedding the luminophores and curing agent in a transparent silicone resin; the mixture was stirred sufficiently to become homogenous and then dispersed on a InGaN chip with 380 nm emitting, and the package was solidified in oven at 120 °C for 40 min.

2.3. Synthesis

2.3.1. General procedure for synthesis of compounds 2a–2d. A solution of nopinone (2 mol) dissolved in ethylene glycol dimethyl ether was added to a suspension of NaH (6 mol) in ethylene glycol dimethyl ether.[43] The mixture was refluxed for 0.5 h, whereupon compounds **1a–1d** (3 mol) dissolved in ethylene glycol dimethyl ether was added to the reaction mixture under reflux. The reacted mixture was quenched by addition of EtOH (95%) after 7 h, and it was extracted with ethyl acetate, and the organic layers were washed with saturated brine to neutrality. After solvent evaporation, the yellow crude crystals were recrystallized from methanol to give **2a–2d**.

Compound **2a** was a pale yellow solid, yield: 69.2%, mp: 127.2–128.8 °C. ^{1}H NMR (400 MHz, $CDCl_3$) δ: 15.61 (s, 1H), 7.64–7.57 (m, 2H), 7.24 (d, J = 8.0 Hz, 2H), 2.70 (dd, J = 3.1, 1.2 Hz, 2H), 2.61–2.49 (m, 2H), 2.40 (s, 3H), 2.28 (tt, J = 6.0, 3.1 Hz, 1H), 1.45 (d, J = 9.5 Hz, 1H), 1.34 (s, 3H), 0.96 (s, 3H). ^{13}C NMR (100 MHz, $CDCl_3$) δ: 209.07, 173.14, 140.50, 132.45, 128.92, 128.16, 103.54, 54.72, 39.91, 39.50, 28.40, 27.80, 25.84, 21.53, 21.48. HRMS (m/z): [M + Na]$^+$ calculated for $C_{17}H_{20}O_2$+Na$^+$, 279.1361; found, 279.1356.

Compound **2b** was a yellow solid, yield: 65.7%, mp: 113.2–113.8 °C. ^{1}H NMR (400 MHz, $CDCl_3$) δ: 15.79 (s, 1H), 7.77–7.68 (m, 2H), 6.97–6.94 (m, 2H), 3.86 (s, 3H), 2.73 (d, J = 3.0 Hz, 2H), 2.60–2.51 (m, 2H), 2.30 (tt, J = 5.7, 2.9 Hz, 1H), 1.46 (d, J = 9.2 Hz, 1H), 1.35 (s, 3H), 0.96 (s, 3H). ^{13}C NMR (100 MHz, $CDCl_3$) δ: 208.76, 172.94, 161.13, 130.05, 127.72, 113.57, 103.09, 55.35, 54.64, 39.99, 39.47, 28.66, 27.86, 25.82, 21.49. HRMS (m/z): [M + Na]$^+$ calculated for $C_{17}H_{20}O_3$+Na$^+$, 295.1310; found, 295.1305.

Compound **2c** was a pale yellow solid, yield: 45.8%, mp: 114.1–114.5 °C. ^{1}H NMR (400 MHz, $CDCl_3$) δ: 15.59 (s, 1H), 7.78–7.65 (m, 2H), 7.20–7.07 (m, 2H), 2.68 (t, J = 2.8 Hz, 2H), 2.66–2.51 (m, 2H), 2.30 (tt, J = 6.0, 3.1 Hz, 1H), 1.45 (d, J = 9.5 Hz, 1H), 1.35 (s, 3H), 0.96 (s, 3H). ^{13}C NMR (100 MHz, $CDCl_3$) δ: 209.24, 171.81, 164.87, 162.38, 130.40, 115.34, 103.72, 54.71, 39.86, 39.54, 28.35, 27.76, 25.80, 21.52. HRMS (m/z): [M + Na]$^+$ calculated for $C_{16}H_{17}FO_2$+Na$^+$, 283.1111; found, 283.1105.

Compound **2d** was a yellow solid, yield: 59.1%, mp: 133.3–133.9 °C. ^{1}H NMR (400 MHz, $CDCl_3$) δ: 15.51 (s, 1H), 7.60 (s, 4H), 2.69 (t, J = 2.9 Hz, 2H), 2.63–2.53 (m, 2H), 2.31 (tt, J = 6.0, 3.1 Hz, 1H), 1.47 (d, J = 9.6 Hz, 1H), 1.37 (s, 3H), 0.98 (s, 3H). ^{13}C NMR (100 MHz, $CDCl_3$) δ: 209.42, 171.40, 134.07, 131.50, 129.79, 124.66, 104.06, 54.77, 39.80, 39.56, 28.26, 27.73, 25.81, 21.55. HRMS (m/z): [M + Na]$^+$ calculated for $C_{16}H_{17}BrO_2$+Na$^+$, 343.0310; found, 343.0304.

2.3.2. General procedure for synthesis of compounds 3a–3d. $BF_3 \cdot (C_2H_5)_2O$ (1.0 mol) was added to a solution of compound **2a–2d** (0.2 mol) in dry dichloromethane, and the reaction mixture was stirred for 2 h at 45 °C. After removal of the solvent, the yellow crude crystals were recrystallized from methanol to give **3a–3d**.

Compound **3a** was a pale yellow solid, yield: 92.6%, mp: 139.3–139.6 °C. ^{1}H NMR (400 MHz, $CDCl_3$) δ: 7.87–7.80 (m, 2H), 7.30 (d, J = 8.1 Hz, 2H), 2.94–2.83 (m, 2H), 2.84–2.74 (m, 1H), 2.68 (dd, J = 11.0, 5.7 Hz, 1H), 2.44 (s, 3H), 1.49 (d, J = 10.1 Hz, 1H), 1.42 (s, 3H), 1.26 (s, 1H), 0.97 (s, 3H). ^{13}C NMR (100 MHz, $CDCl_3$) δ: 201.83, 179.42, 144.19, 130.60, 129.62, 129.33, 104.19, 51.25, 40.39, 39.79, 28.49, 28.41, 25.49, 21.72, 21.42. HRMS (m/z): [M + Na]$^+$ calculated for $C_{17}H_{19}BF_2O_2$+Na$^+$, 327.1344; found, 327.1341.

Compound **3b** was a yellow solid, yield: 89.3%, mp: 147.7–148.2 °C. ^{1}H NMR (400 MHz, $CDCl_3$) δ: 8.04–7.96 (m, 2H), 7.04–6.92 (m, 2H), 3.90 (s, 3H), 2.89 (dd, J = 14.6, 3.0 Hz, 2H), 2.77 (t, J = 5.6 Hz, 1H), 2.73–2.60 (m, 1H), 2.42 (tt, J = 5.9, 3.0 Hz, 1H), 1.49 (d, J = 10.0 Hz, 1H), 1.42 (s, 3H), 0.97 (s, 3H). ^{13}C NMR (100 MHz, $CDCl_3$) δ: 200.80, 178.45, 163.72, 132.26, 125.68, 114.05, 103.54, 55.61, 51.17, 40.31, 39.90, 28.80, 28.57, 25.50, 21.39. HRMS (m/z): $[M + Na]^+$ calculated for $C_{17}H_{19}BF_2O_3$+Na^+, 343.1293; found, 343.1291.

Compound **3c** was a white solid, yield: 81.9%, mp: 160.2–160.8 °C. ^{1}H NMR (400 MHz, $CDCl_3$) δ: 8.04–7.92 (m, 2H), 7.25–7.12 (m, 2H), 2.92–2.78 (m, 3H), 2.70 (dd, J = 10.5, 5.8 Hz, 1H), 2.43 (tt, J = 5.9, 3.0 Hz, 1H), 1.50 (d, J = 10.2 Hz, 1H), 1.43 (s, 3H), 0.97 (s, 3H). ^{13}C NMR (100 MHz, $CDCl_3$) δ: 202.81, 177.96, 166.66, 164.11, 132.13, 129.57, 115.94, 104.22, 51.38, 40.49, 39.75, 28.39, 25.47, 21.42. HRMS (m/z): $[M + Na]^+$ calculated for $C_{16}H_{16}BF_3O_2$+Na^+, 331.1093; found, 331.1091.

Compound **3d** was a yellow solid, yield: 86.9%, mp: 175.2–175.7 °C. ^{1}H NMR (400 MHz, $CDCl_3$) δ: 7.83–7.74 (m, 2H), 7.69–7.59 (m, 2H) 2.91–2.75 (m, 3H), 2.71 (dd, J = 10.6,5.8 Hz, 1H), 2.43 (tt, J = 5.9, 3.1 Hz, 1H), 1.49 (d, J = 10.2 Hz, 1H), 1.43 (s, 3H), 0.97 (s, 3H). ^{13}C NMR (100 MHz, $CDCl_3$) δ: 203.26, 178.01, 132.21, 131.97, 130.81, 128.07, 104.57, 51.45, 40.56, 39.71, 28.41, 28.20, 25.50, 21.47. HRMS (m/z): $[M + Na]^+$ calculated for $C_{16}H_{16}BBrF_2O_2$+Na^+, 391.0293; found, 391.0290.

3. Results and discussion

3.1. Synthesis

The synthetic routines of four fluorescent compounds were shown in Scheme 1. The compounds **2a–2d** were prepared from nopinone and compounds **1a–1d** according to the Claisen condensation. Target compounds **3a–3d** were then synthesized by reaction of compounds **2a–2d** with $BF_3{\cdot}(C_2H_5)_2O$ with high yields. The chemical structures of the synthesized compounds were confirmed by ^{1}H NMR, ^{13}C NMR, and HRMS. Compounds were readily soluble in common organic solvents like THF, chloroform, ethyl acetate. The structure of **2a** was also verified by X-ray crystallography (Fig. S1†). Suitable single crystals of **2a** for X-ray structural analysis was obtained by slow evaporation of methanol solution at room temperature.

3.2. Photophysical properties

The photophysical properties of the resultant compounds **3a–3d** in neat film were investigated. The UV-vis absorption spectra of **3a–3d** at room temperature are shown in Fig. 1. The compounds **3c**, **3a**, **3d**, **3b**, exhibited a strong absorption maximum in neat film at 366 nm to 368 nm, 374 nm, and 388 nm, respectively. The photoluminescence (PL) spectra of **3a–3d** at room temperature are shown in Fig. 1. All obtained compounds showed obvious fluorescence emission (emission maxima λ_{em} = 496 nm for **3b** *vs.* 480 nm for **3d**, 463 nm for **3a**, and 441 nm for **3c**, Table 1), which can be ascribed to the different electron density dispersed on the molecules. Obviously, compound **3c** showed bathochromic shift due to the presence of electron-donating methoxy, which enhanced

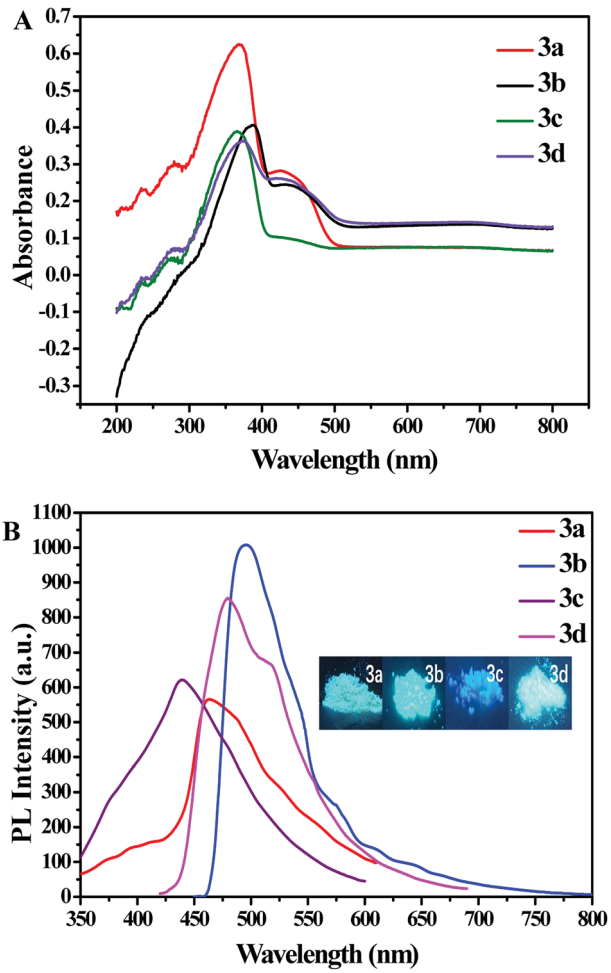

Fig. 1 (A) Absorbance spectra and (B) emission spectra of **3a–3d** in neat film at room temperature. Inset: Photographs of **3a–3d** under 365 nm UV light illumination.

intramolecular charge transfer (ICT) process between the electron-donating methoxy and the electron-accepting BF_2dbm unit, and led to shift the λ_{max} to the long wavelength. The ICT process of these compounds were further studied in both experimental investigation (Fig. S2†) and theoretical calculation (Fig. 2).

The absolute photoluminescence quantum yields for compounds **3a–3d** in solid state are summarized in Table 1, and the values of compounds **3a–3d** were 1.99%, 47.16%, 4.94% and 21.03%, respectively. It was found that introduction of methyl, fluorine, bromine moiety did not make an obvious difference in

Table 1 Photophysical data of **3a–3d**

Compound	λ_{abs} (nm)	λ_{em} (nm)	Φ_F [a]	τ_F (ns)	K_f [b] (10^9 s^{-1})	K_{nr} [c] (10^9 s^{-1})
3a	368	463	1.99%	1.52	0.01	0.64
3b	388	496	37.16%	4.52	0.08	0.14
3c	366	441	4.94%	1.10	0.04	0.86
3b	374	480	12.03%	2.15	0.06	0.41

[a] Φ_F is the absolute photoluminescence quantum yields. [b] Radiative rate constant ($k_f = \Phi_f/\tau_f$). [c] Non radiative rate constant ($k_{nr} = (1 - \Phi_f)/\tau_f$).

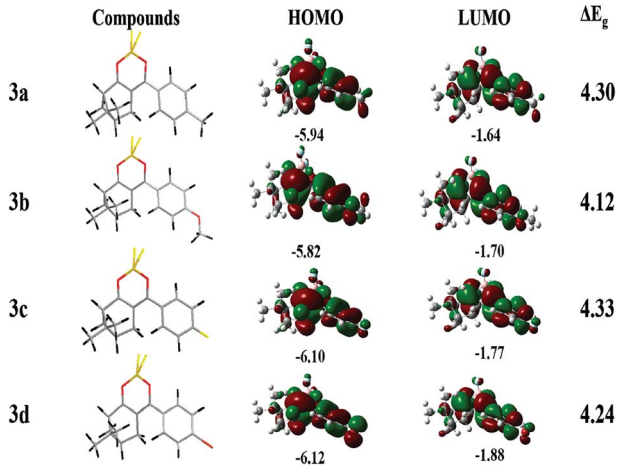

Fig. 2 HOMO and LUMO diagrams of **3a–3d**.

terms of the fluorescence lifetime (**3a**, $\tau_f = 1.52$ ns; **3c**, $\tau_f = 1.10$ ns; **3d**, $\tau_f = 2.15$ ns). However, compared with other compounds, the fluorescence lifetime of **3b** substituted with methoxy has increased by 2 times (**3b**, $\tau_f = 4.52$ ns). Based on fluorescence lifetimes of these compounds, radiative and non-radiative rate constants (k_f and k_{nr}) were respectively estimated.[44,45] As shown in Table 1, methoxy group increased the k_f (the radiative rate constant) and decreased the k_{nr} (the non-radiative rate constant) of BF_2 complexes. Thus, the introduction of different substituent functional groups can significantly affect the photoluminescence properties of BF_2 complexes.

3.3. Electrochemical properties and theoretical calculations

The electrochemical properties of **3a–3d** were examined using cyclic voltammetry. The cyclic voltammograms of the **3a–3d** are shown in Fig. S2,† the onset oxidation potentials (E_{OX}) were found to be 1.30, 1.26, 1.34 and 1.35 V for compounds **3a–3d**. According to the equation [HOMO = −(4.40 + E_{OX})], the HOMO energy levels were calculated. The lowest unoccupied molecular orbital energy levels (E_{LUMO}) is calculated based on the equation of $E_{LUMO} = E_{HOMO} + E_g$, in which energy band gap (E_g = 4.1 eV for **3a**, 3.89 eV for **3b**, 4.11 eV for **3c** and 4.05 eV for **3d**, respectively) were estimated from the UV-vis absorption. HOMO–LUMO gap is usually used to characterize the ICT occurred in chromophore molecules. The HOMO, LUMO and E_g are listed in Table 2. The CV curves of these compounds remained unchanged under multiple successive scans, demonstrating their good stability against electrochemical oxidation.

To further investigate the relationship between the emission and the structure property of the four compounds at the molecular level, the geometrical structures of compounds **3a–3d** were analyzed employing DFT calculations. The electron density distributions of target compounds are illustrated in Fig. 2. The electron clouds of the HOMOs and LOMOs for **3a**, **3c**, **3d** were mainly distributed over whole molecule. The electron clouds of the HOMOs in **3b** were mainly distributed over the whole molecule, and the electron clouds of the LUMOs were mostly distributed over BF_2dbm unit due to electron withdrawing ability of the BF_2dbm unit. These results further prove that the ICT process occurs from the donor to the acceptor moiety. The corresponded data are summarized in Table 2. According to the calculations, introduction of methoxy may reduce the HOMO–LUMO energy gap (4.12 eV for **3b**, 4.24 eV for **3d**, 4.3 eV for **3a** and 4.33 eV for **3c**, respectively) which is consistent with the results of cyclic voltammetry. The HOMO and LUMO gap of compound **3b** is lower than that of **3a**, **3c**, **3d**, which could lead to a red-shift in the absorption and fluorescence spectra. The conclusion is coincident with the experimental results.

Table 2 Electrochemical properties and thermostability of **3a–3d**

	HOMO (eV)		LUMO (eV)		E_g (eV)		
Compounds	Exptl[a]	Calc	Exptl[a]	Calc	Exptl[b]	Calc	T_d (°C)
3a	5.70	−5.94	−1.60	−1.64	4.10	4.30	252.3
3b	5.66	−5.82	−1.77	−1.70	3.89	4.12	296.6
3c	5.74	−6.10	−1.63	−1.77	4.11	4.33	232.8
3d	5.75	−6.12	−1.70	−1.88	4.05	4.24	285.4

[a] Estimated from HOMO = −(4.4 + E_{OX}); LUMO = HOMO + E_g. [b] Estimated from the onset of the absorption spectra.

3.4. Thermal properties

The thermal stabilities of four new compounds were evaluated by thermogravimetric analysis (TGA) under a stream of N_2 with a scanning rate of 10 °C min^{-1}. Their TGA curves are shown in Fig. S3† and their degradation temperatures (T_d) for 5% weight loss are listed in Table 2. The degradation temperatures T_d for compounds **3a–3d** were 252.3, 296.6, 232.8 and 285.4 °C, respectively. The data demonstrate that the resulting compounds can possess good thermal properties, which is desirable for the application in electroluminescent materials.

3.5. Aggregation-induced emission performances

The PL emission spectra of resultant compounds **3a–3d** in DMF/water mixtures with different water fractions (f_w: 0–90%) in Fig. S4–S6,† Fig. 3 reveals that the PL intensity of **3b** is slightly weakened upon addition of a small amount of water ($f_w \leq 20\%$) and the dramatic enhancement of luminescence is observed for the water fraction (f_w) of 30%. Similar observation is seen for **3c**, **3a** and **3d**. All compounds showed higher emission intensity when water fractions (f_w) was 90%.

According to the Fig. S7,† the emission of **3b** is weaker in pure DMF solution owing to the twisted intramolecular charger transfer (TICT) emission. The emission spectra remained almost unchanged when the water volume fraction was gradually increased from 0% to 20%. When the water content was further increased from 30% to 90%, the fluorescence intensity was swiftly enhanced, which attributed to the restriction of intramolecular rotation (RIR)[46–48] According to the Fig. S7,† the emission of **3b** in the water fraction (f_w) of 60% is weaker than that of 50%, which is probably due to the difference in aggregate morphology.[49,50] It is obvious that the poor solvent water could induce the fluorescence intensity increase, demonstrating the AIE characteristics of the four compounds.

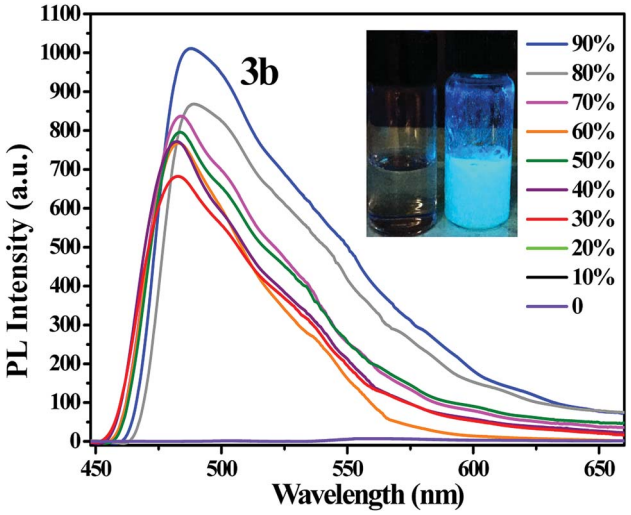

Fig. 3 PL spectra of **3b** in DMF/water mixtures with different water fractions. Inset: Photographs of **3b** in DMF/water mixtures (f_w = 0% and 90%), taken under 365 nm UV light illumination.

3.6. Electroluminescent devices

Owing to relatively high absolute fluorescence quantum yields of **3b** and **3d**, EL devices based on **3b** and **3d** were fabricated. As shown in Fig. 4 and Fig. S8,† both of the devices I and II display blueish-green light (peak at 499.2 nm and peak at 500.4 nm, respectively), the Commission Internationale de L'Eclairage (CIE) coordinates of devices I and devices II are located at (0.2774, 0.4531) and (0.3084, 0.4800) respectively, which are close to their solid PL spectra.

As showed in Fig. 5 and Table 3, the EL performances of the luminescent materials substituted with methoxy was better than the luminescent materials substituted with bromine, which is identical to the order of photophysical properties in the solid state. For the device of I, a luminous efficacy (η_p) of 7.09 lm W^{-1}, a color rendering index (R_a) of 54.4 and a correlated color temperature (T_C) of 7028 K at a current density of 9.9 mA were achieved. Therefore, the nopinone derivative containing difluoroboron is still one effective strategy for new EL materials.

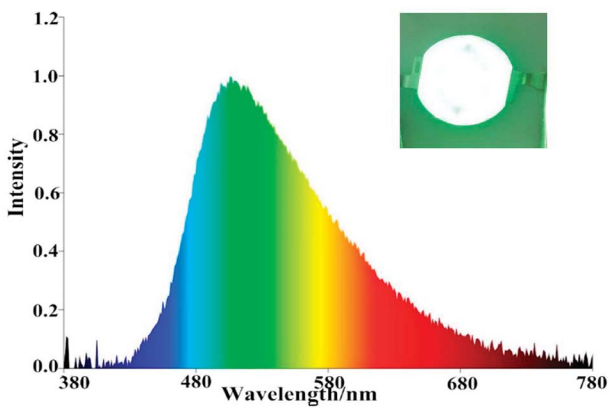

Fig. 4 EL spectra of device I (**3b**). Inset: Photographs of device I (**3b**) at a current density of 9.9 mA.

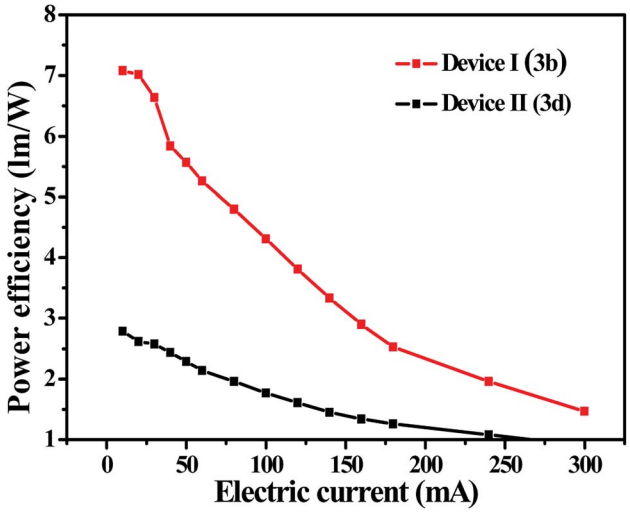

Fig. 5 The electric current–power efficiency curves of the device I (**3b**) and II (**3d**).

Table 3 Electroluminescence properties of device I (**3b**) and II (**3d**)

Device	V_F (V)	EL (nm)	η_p (lm W^{-1})	T_C (K)	CIE (x, y)	R_a
I	3.075	499.2	7.08	7028	(0.2774, 0.4531)	54.4
II	3.06	500.4	2.79	6087	(0.3084, 0.4800)	55.4

4. Conclusions

In summary, four novel nopinone derivative containing difluoroboron β-diketonate groups **3a–3d** were synthesized with a simple method. The photophysical experiments demonstrated that the maximum absorption wavelengths of new compounds were in the range of 360–390 nm and the maximum fluorescence wavelengths of new compounds were in the range of 440–500 nm. These compounds also exhibited emission enhancement in their aggregate state. Besides, four target compounds **3a–3d** exhibited high thermal stabilities, which is necessary for fabricating long lifetime devices. Theoretical calculations (DFT) were performed to provide further insights into our experimental results. Furthermore, devices I and II were fabricated which displayed blueish-green EL emission (peak at 499.2 nm and 500.4 nm, respectively). Among the two devices, the device of I exhibited the highest device performance with a luminous efficacy (η_p) of 7.09 lm W^{-1}, a color rendering index (R_a) of 54.4 and a correlated color temperature (T_C) of 7028 K, which provide guidance for the design and synthesis of new efficient EL materials in the future.

Conflicts of interest

There are no conflicts to declare.

Acknowledgements

The research was supported by the National Natural Science Foundation of China (No. 31470592), the Natural Science

Foundation of Jiangsu Province (Grants No. BK20151513), Jiangsu Provincial Key Lab for the Chemistry and Utilization of Agro-Forest Biomass, and Priority Academic Program Development of Jiangsu Higher Education Institutions, China.

References

1 A. Kamkaew, S. H. Lim and H. B. Lee, *Chem. Soc. Rev.*, 2013, **42**, 77–88.
2 N. Boens, V. Leen and W. Dehaen, *Chem. Soc. Rev.*, 2012, **41**, 1130–1172.
3 F. Cardona, J. Rocha and A. M. S Silva, *Dyes Pigm.*, 2014, **111**, 16–20.
4 S. Guieu, F. Cardona and J. Rocha, *New J. Chem.*, 2014, **38**, 5411–5414.
5 S. Xu, R. E. Evans and T. Liu, *Inorg. Chem.*, 2013, **52**, 3597–3610.
6 P. Galer, R. C. Korošec and M. Vidmar, *J. Am. Chem. Soc.*, 2014, **136**, 7383–7394.
7 S. Guieu, J. Pinto and V. L. M. Silva, *Eur. J. Org. Chem.*, 2015, 3423–3426.
8 H. Zhang, C. Liu and J. Xiu, *Dyes Pigm.*, 2017, **136**, 798–806.
9 C. T. Poon, W. H. Lam and H. L. Wong, *J. Am. Chem. Soc.*, 2010, **132**, 13992–13993.
10 A. D'Aléo, D. Gachet and V. Heresanu, *Chem.– Eur. J*, 2012, **18**, 12764–12772.
11 H. X. Zhang, J. B. Chen and X. F. Guo, *Anal. Chem.*, 2014, **86**, 3115–3121.
12 W. Liu, F. Li and X. Chen, *J. Am. Chem. Soc.*, 2014, **136**, 4468–4471.
13 Y. Zhou, Y. Z. Chen and J. H. Cao, *Dyes Pigm.*, 2015, **112**, 162–169.
14 S. Chambon, A. D'Aléo and C. Baffert, *Chem. Commun.*, 2013, **49**, 3555–3557.
15 G. Q. Zhang and J. B. Chen, *J. Am. Chem. Soc.*, 2007, **129**, 8942–8943.
16 G. Zhang, J. Lu and M. Sabat, *J. Am. Chem. Soc.*, 2010, **132**, 2160–2162.
17 M. Y. Liu, Z. Lu and J. B. Sun, *Dyes Pigm.*, 2016, **128**, 271–278.
18 I. García-Moreno, F. Amat-Guerri and M. Liras, *Adv. Funct. Mater.*, 2010, **17**, 3088–3098.
19 H. Maeda, T. Shirai and S. Uemura, *Chem. Commun.*, 2013, **49**, 5310–5312.
20 R. Yamaka, T. Sakurai and W. Matsuda, *Chem.– Eur. J*, 2016, **22**, 626–638.
21 X. Sun, X. Zhang and X. Li, *J. Mater. Chem.*, 2012, **22**, 17332–17339.
22 Q. Chong, M. Y. Liu and G. H. Hong, *Org. Biomol. Chem.*, 2015, **13**, 2986–2991.
23 C. A. Derosa and Z. Fan, *Macromolecules*, 2015, **48**, 2967–2977.
24 J. Samonina-Kosicka, C. A. Derosa and W. A. Morris, *Macromolecules*, 2014, **47**, 3736–3746.
25 J. D. Luo, Z. L. Xie and B. Z. Tang, *Chem. Commun.*, 2001, **18**, 1740–1741.
26 B. Xu, J. He and Y. Mu, *Chem. Sci.*, 2015, **6**, 3236–3241.
27 M. Luo, X. Zhou and Z. Chi, *Dyes Pigm.*, 2014, **101**, 74–84.
28 Z. Zhao, W. Y. L. Lam and B. Z. Tang, *J. Mater. Chem.*, 2012, **22**, 23726–23740.
29 J. Yang, N. Sun and J. Huang, *J. Mater. Chem. C*, 2015, **3**, 2624–2631.
30 L. Chen, Y. Jiang and H. Nie, *Adv. Funct. Mater.*, 2014, **24**, 3621–3630.
31 J. Mei, J. Wang and J. Z. Sun, *Chem. Sci.*, 2012, **3**, 549–558.
32 S. Choi, J. Bouffard and Y. Kim, *Chem. Sci.*, 2013, **5**, 751–755.
33 R. Hu, C. F. Gómez-Durán and J. W. Lam, *Chem. Commun.*, 2012, **48**, 10099–10101.
34 C. Liu, W. He and G. Shi, *Dyes Pigm.*, 2015, **112**, 154–161.
35 X. Zhang, Z. Chi and B. Xu, *J. Mater. Chem.*, 2012, **22**, 18505–18513.
36 Y. Guo, X. Feng and T. Han, *J. Am. Chem. Soc.*, 2014, **136**, 15485–15488.
37 S. Kaur, A. Gupta and V. Bhalla, *J. Mater. Chem. C*, 2014, **2**, 7356–7363.
38 Z. Zheng, Z. Yu and M. Yang, *J. Org. Chem.*, 2013, **78**, 3222–3234.
39 S. Liao, S. Shang and M. Shen, *Bioorg. Med. Chem. Lett.*, 2016, **26**, 1512–1515.
40 Z. Szakonyi, T. Gonda and F. Fülöp, *Tetrahedron: Asymmetry*, 2014, **25**, 1138–1145.
41 J. Ścianowski, J. Szumera and P. Kleman, *Tetrahedron: Asymmetry*, 2016, **27**, 238–245.
42 J. Yang, H. Xu and X. Xu, *Dyes Pigm.*, 2016, **128**, 75–85.
43 T. Wu and X. You, *J. Phys. Chem. A*, 2012, **116**, 8959–8964.
44 M. Lin, Y. Yu and L. Li, *Org. Electron.*, 2018, **57**, 123–132.
45 H. Liu, Z. Lu and B. Tang, *Dyes Pigm.*, 2018, **149**, 284–289.
46 G. W. Kim, D. R. Yang and C. K. Yong, *Dyes Pigm.*, 2016, **136**, 8–16.
47 H. Dong, M. Luo and S. Wang, *Dyes Pigm.*, 2016, **139**, 118–128.
48 C. Li, W. Yang and W. Zhou, *New J. Chem.*, 2016, **40**, 8837–8845.
49 F. Zhang, Y. Guan and S. Wang, *Dyes Pigm.*, 2016, **130**, 1–8.
50 W. Li, T. Xu and G. Chen, *Dyes Pigm.*, 2018, **149**, 266–272.

